



Research article

Application of acid-activated Bauxsol for wastewater treatment with high phosphate concentration: Characterization, adsorption optimization, and desorption behaviors



Jie Ye ^{a, b, c}, Xiangna Cong ^d, Panyue Zhang ^{a, b, *}, Guangming Zeng ^{a, b, **},
 Erhard Hoffmann ^c, Yang Liu ^{a, b}, Yan Wu ^{a, b}, Haibo Zhang ^{a, b}, Wei Fang ^{a, b},
 Hermann H. Hahn ^c

^a College of Environmental Science and Engineering, Hunan University, Changsha 410082, PR China

^b Key Laboratory of Environmental Biology and Pollution Control (Hunan University), Ministry of Education, Changsha 410082, PR China

^c Department of Aquatic Environmental Engineering, Karlsruhe Institute of Technology, Karlsruhe D-76131, Germany

^d The Institute for Applied Materials IAM-WK, Karlsruhe Institute of Technology, Karlsruhe D-76131, Germany

ARTICLE INFO

Article history:

Received 18 August 2015

Received in revised form

24 October 2015

Accepted 9 November 2015

Available online xxx

Keywords:

Red mud

Activation

Structure change

Central composite design

Desorption

ABSTRACT

Acid-activated Bauxsol was applied to treat wastewater with high phosphate concentration in a batch adsorption system in this paper. The effect of acid activation on the change of Bauxsol structure was systematically investigated. The mineralogical inhomogeneity and intensity of Bauxsol decreased after acid activation, and $\text{FeCl}_3 \cdot 2\text{H}_2\text{O}$ and $\text{Al}(\text{OH})_3$ became the dominant phases of acid-activated Bauxsol adsorption. Moreover, the BET surface area and total pore volume of Bauxsol increased after acid activation. Interaction of initial solution pH and adsorption temperature on phosphate adsorption onto acid-activated Bauxsol was investigated by using response surface methodology with central composite design. The maximum phosphate adsorption capacity of 192.94 mg g^{-1} was achieved with an initial solution pH of 4.19 and an adsorption temperature of $52.18 \text{ }^\circ\text{C}$, which increased by 7.61 times compared with that of Bauxsol (22.40 mg g^{-1}), and was higher than other adsorbents. Furthermore, the desorption studies demonstrated that the acid-activated Bauxsol was successfully regenerated with 0.5 mol L^{-1} HCl solution. The adsorption capacity and desorption efficiency of acid-activated Bauxsol maintained at 80.48% and 93.02% in the fifth adsorption–desorption cycle, respectively, suggesting that the acid-activated Bauxsol could be repeatedly used in wastewater treatment with high phosphate concentration.

© 2015 Elsevier Ltd. All rights reserved.

1. Introduction

Phosphorus is one of the most important environmental pollutants with high concentration in industrial wastewater. Sohsalam and Sirianuntapiboon (2008) found that the phosphorus concentration in molasses wastewater was higher than 225 mg L^{-1} . Shao

et al. (2008) showed that the concentration of total phosphorus in brewery slurry was about $144\text{--}216 \text{ mg L}^{-1}$. Chowdhury et al. (2010) concluded that the phosphate concentration in fish processing wastewater reached $10\text{--}390 \text{ mg L}^{-1}$. The accumulation of phosphate compounds resulted from discharge of untreated industrial wastewater can lead to eutrophication in water bodies with potential threat to both aquatic ecosystems and human health (Yao et al., 2013). Therefore, there is an urgent need to develop simple and cost-effective treatment methods for industrial wastewater containing high phosphate concentration.

Many conventional and novel methods, including adsorption, precipitation, ion exchange, and electrodialysis, have been widely employed to remove and recover phosphate from industrial wastewater (Xu et al., 2012; Weng et al., 2011; Zhang et al., 2010; Gong et al., 2009; Oguz, 2004). Among them, adsorption method is believed to be one of the most economical, effective, and reliable

* Corresponding author. College of Environmental Science and Engineering, Hunan University, Yuelushan, Changsha 410082, China.

** Corresponding author. College of Environmental Science and Engineering, Hunan University, Yuelushan, Changsha 410082, China.

E-mail addresses: eyejie@126.com (J. Ye), Xiangnacong@hotmail.com (X. Cong), zhangpanyue@hnu.edu.cn (P. Zhang), zgming@hnu.edu.cn (G. Zeng), erhard.hoffmann@kit.edu (E. Hoffmann), jungsten@163.com (Y. Liu), wuyan19850827@hotmail.com (Y. Wu), haibo_zhang@hnu.edu.cn (H. Zhang), fw8905@163.com (W. Fang), hermann.hahn@kit.edu (H.H. Hahn).

methods. It provides the possibility of recovering the phosphate by desorption and using the phosphate-loaded adsorbents in agriculture as phosphate fertilizer and soil conditioner (Zhang et al., 2010). Various natural minerals, industrial by-products and synthetic adsorbents have been used in phosphate adsorption systems. Among these available materials, red mud is considered to be a promising alternative (Gadepalle et al., 2007; Lombi et al., 2002).

Red mud is a solid waste residue formed after the caustic digestion of bauxite ores during the alumina production, which has got a variety of applications due to its specific physicochemical characteristics such as high contents of Fe and Al (Pérez-Villarejo et al., 2012; Bhatnagar et al., 2011; Castaldi et al., 2010; Liu et al., 2009; Yang et al., 2008). In order to further improve the adsorption performance of red mud, the modification of red mud has become an emerging and promising research field (Yue et al., 2010; Huang et al., 2008). The neutralized red mud (Bauxsol), a modified product of red mud, has many advantages for pollutants removal including high surface/volume ratios, and excellent adsorption performance (Despland et al., 2010). In recent years, acid activation after neutralization of red mud has been proven to be effective for further improving the physicochemical characters of red mud. For instance, Genç-Fuhrman et al. (2004, 2005) demonstrated that the acid-activated Bauxsol had good adsorption potential for arsenate removal in the batch and fixed-bed studies. Tor et al. (2009) reported that the phenol adsorption capacity of neutralized red mud significantly increased after acid activation. In our previous study, acid-activated Bauxsol has been proven to be an effective adsorbent for phosphate removal (Ye et al., 2014).

Most previous studies were focused on the optimization of acid activation conditions, the exact role of acid activation is not well documented. Genç-Fuhrman et al. (2004) considered that acid activation process cleaned the effective adsorption sites on adsorbent surface, while Freire et al. (2012) found that the addition of acid solution resulted in dissolution of partial minerals and increase of surface protonation. The effect of acid activation process on change of Bauxsol structure is still unclear. Meanwhile, few studies on the effect and interaction of different operational adsorption factors on the adsorption process of acid-activated Bauxsol have been reported. Therefore, the specific objectives of this study were: (1) analyzing the effect of acid activation on change of Bauxsol structure; (2) investigating the influence of initial solution pH and adsorption temperature on phosphate removal by acid-activated Bauxsol using central composite design (CCD); (3) conducting multiple adsorption–desorption cycles to investigate the reusability of acid-activated Bauxsol in treating wastewater with high phosphate concentration.

2. Materials and methods

2.1. Materials

Acid-activated Bauxsol was prepared by the methods reported in Ye et al. (2014). For operation convenience, in this research the HCl concentration, activation temperature and activation time were chosen as 10.00 mol L⁻¹, 40.00 °C, and 5.00 h, respectively. The phosphate solution was prepared by KH₂PO₄, which was of analytical grade (Merck, Germany).

2.2. Characterization of Bauxsol samples

The surface micro-morphology of acid-activated Bauxsol were analyzed with an electron dispersive X-ray analysis (OXFORD X-Max, Oxford Instruments, UK), which was coupled with an electronic detector (LEO 1530, LEO, Germany). The X-ray photoelectron spectroscopy (XPS) measurement was performed using an X-ray

photoelectron spectrometer (Escalab 250Xi, Thermo Scientific, UK) equipped with Al K α radiation (1486.6 eV) to determine the elemental composition on the surface of acid-activated Bauxsol. The specific surface area and pore size distribution of Bauxsol samples were obtained by nitrogen gas sorption method (ASAP 2020 V3.04 H, Micromeritics, USA). The chemical composition of Bauxsol samples was determined by X-Ray Fluorescence Spectrometer (S4 Explorer, Bruker, Germany). The Fourier transform infrared (FTIR) spectra of Bauxsol samples were recorded at room temperature using a FTIR Spectrometer (MAGNA FTIR 750, Nicolet, USA) in 400–4000 cm⁻¹ region. The KBr (FTIR grade, Fluka) was dried at 200 °C for 24 h and used for FTIR measurement. The XRD patterns of Bauxsol samples were detected using an X-ray diffractometer (XRD-6000, Shimadzu, Japan) with Cu K α radiation at 40 kV and 30 mA, and recorded in a 2 θ range of 10–70° at a scan speed range of 0.02° s⁻¹.

2.3. Adsorption studies

In order to investigate the potential of acid-activated Bauxsol for treating industrial wastewater with high phosphate concentration, the initial phosphate concentration was chosen as 200 mg L⁻¹. The pH of phosphate solutions was adjusted with 1 mol L⁻¹ and 0.1 mol L⁻¹ HCl or NaOH solution. The adsorption temperature was controlled with a gyratory water bath shaker (model G76, New Brunswick Scientific, USA). Adsorption studies were carried out in beaker flasks with the acid-activated Bauxsol dosage of 0.5 g L⁻¹. The flasks were shaken at 100 r min⁻¹ for 2 h. The equilibrium duration of 2 h was determined by the preliminary experiments. After adsorption equilibrium, the sample was centrifuged at 3000 r min⁻¹ for 1 min, and the supernatant was taken to analyze the phosphate concentration.

The phosphate adsorbed by per unit of adsorbent was calculated by Eq. (1):

$$q = \frac{(C_i - C_f) \cdot V}{m} \quad (1)$$

where q is the phosphate adsorption capacity per unit of acid-activated Bauxsol (mg g⁻¹), C_i and C_f are the initial and final phosphate concentration (mg L⁻¹), respectively, V is the solution volume (L), and m is the mass of adsorbent (g).

The pH value was measured with a multimeter (model Multiline P4, WTW, Germany). The phosphate concentration was determined via the spectrophotometric method DIN-EN-ISO-15681-1 with a QuikChem 8500 flow injection analysis system (Lachat Instruments, USA). All experiments were conducted in triplicate and the average values were used for data analysis.

2.4. Experimental design for optimization of adsorption factors

Preliminary experiments with one-factor-at-a-time method were done to find out important operational factors influencing the phosphate adsorption onto acid-activated Bauxsol and to determine a narrow range of them. Results showed that the initial solution pH and adsorption temperature were the important operational factors.

Response surface methodology (RSM) is a collection of statistical and mathematical technique for developing, improving, and optimizing process (Talebpour et al., 2009), which is a valuable tool to investigate the interaction between factors and to depict the effects of given factors on their measured responses quantitatively (Hatambeygi et al., 2011; Bezerra et al., 2008). In this research the RSM with central composite design (CCD) was applied for further

optimization of operational factors. Each variation was coded at five levels: $-\alpha$, -1 , 0 , $+1$, $+\alpha$. Here the value of α was coded as 1.414 according to program setting. The design and analysis of variations were evaluated using Design-Expert V8.0. The quadratic equation model for predicting the optimal conditions with CCD is expressed as Eq. (2):

$$Y = \beta_0 + \sum_{i=1}^k \beta_i X_i + \sum_{i=1}^k \beta_{ii} X_i^2 + \sum_{i < j}^k \sum_j^k \beta_{ij} X_i X_j + \dots + e \quad (2)$$

where Y is the predicted response, X_i, X_j, \dots, X_k are the input variables, which affect the response Y , $X_i^2, X_j^2, \dots, X_k^2$ are the square effects, $X_i X_j, X_i X_k$ and $X_j X_k$ are the interaction effects, β_0 is the intercept, $\beta_i (i = 1, 2, \dots, k)$ is the linear effect, $\beta_{ii} (i = 1, 2, \dots, k)$ is the squared effect, $\beta_{ij} (i = 1, 2, \dots, k; j = 1, 2, \dots, k)$ is the interaction effect and e is a random error (Kunamneni and Singh, 2005).

In a dependent-independent variable modeling approach, it is necessary to assess the relative importance and contribution of each independent variable in a model (Desai et al., 2008). In this study, the Pareto values (P) were chosen to assess the significance and contribution of initial solution pH and adsorption temperature in RSM model. It was calculated by Eq. (3) (Haaland, 1989):

$$P_i = \left(\frac{\beta_i^2}{\sum_{i=1}^k \beta_i^2} \right) \quad (3)$$

2.5. Desorption studies

After adsorption equilibrium with certain experimental conditions (acid-activated Bauxsol dosage: 0.5 g L^{-1} ; initial phosphate concentration: 200 mg L^{-1} ; initial solution pH: 4.5; adsorption temperature, $50 \text{ }^\circ\text{C}$; agitation speed, 100 r min^{-1}), the acid-activated Bauxsol adsorbed with phosphate was separated from the solution by filtration and then added into 50 mL HCl solution of 0.5 mol L^{-1} . After stirring at 100 r min^{-1} and $50 \text{ }^\circ\text{C}$ for 60 min , the phosphate concentration of supernatant was determined. After each cycle of adsorption–desorption, adsorbent was washed with distilled water and used in the succeeding cycle. Five cycles were implemented successively.

Desorption efficiency was defined as Eq. (4):

$$\text{Desorption efficiency (\%)} = \frac{\text{desorbed amount of phosphate}}{\text{adsorbed amount of phosphate}} \times 100 \quad (4)$$

3. Results and discussion

3.1. Effect of acid activation on change of Bauxsol structure

Surface property of Bauxsol before and after acid activation is shown in Table 1. It was found that acid-activated Bauxsol displayed a larger BET surface area and total pore volume than Bauxsol. The analysis of pore size distribution illustrated that more mesopores were formed on the surface after acid activation (as shown in Fig. S1). The results were consistent with that reported by Genç-

Fuhrman et al. (2004), who contribute the larger BET surface area and total pore volume to the cleaning of effective adsorption sites on adsorbent surface with acid activation.

The XPS spectra of acid-activated Bauxsol demonstrated that different elements including iron (Fe), aluminum (Al), oxygen (O), silicon (Si), titanium (Ti) and carbon (C) were detected on the surface (as shown in Fig. S2). The chemical composition of Bauxsol samples before and after acid activation is listed in Table 2, which shows that Fe and Al oxides are the main components of both Bauxsol and acid-activated Bauxsol. Meanwhile, it should be pointed out that the percentage of Fe oxide decreased from 47.13% to 33.88% after acid activation, suggesting possible transformation of minerals containing Fe element.

FTIR spectra of Bauxsol samples before and after acid activation are shown in Fig. 1. A strong and broad band in $3600\text{--}3100 \text{ cm}^{-1}$ region (O–H stretching vibration) should be assigned for the presence of hydroxyl of coordinate water molecules (Zhou et al., 2011; Long et al., 2011; Savii et al., 2002), and a band at 1635 cm^{-1} (O–H bending vibration) was assigned to the deformation of water molecules, indicating the presence of physisorbed water on the samples (Yu et al., 2007; Ivanova et al., 2001). The adsorption bands at 1467 cm^{-1} (C=O stretching vibration) and 999 cm^{-1} (C–O stretching vibration) disappeared after acid activation (Jangir et al., 2010), confirmed the reaction of CO_3^{2-} groups with HCl solution. The peaks at 903 cm^{-1} and 801 cm^{-1} was displaced by a new peaks at 1100 cm^{-1} , which was assigned to Si–O vibrations of amorphous silica with a three-dimensional framework originated from acid treatment (Siriwardane et al., 2007; Parikh and Chorover, 2006). More importantly, the intensity of peak at 471 cm^{-1} , attributing to stretching vibrations of Fe–O bonds, weakened significantly after acid activation, suggesting the possible dissolution of Fe oxides/hydroxides like Fe_2O_3 (Gok et al., 2007).

Fig. 2 shows X-ray diffraction patterns of Bauxsol samples before and after acid activation. Bauxsol presented specific chemical composition diffraction peaks at different 2θ ($^\circ$), indicating the presence of goethite ($\text{FeO}(\text{OH})$), hematite (Fe_2O_3), gibbsite ($\text{Al}(\text{OH})_3$), anatase (TiO_2) and quartz (SiO_2). The peaks of hematite (Fe_2O_3) and goethite ($\text{FeO}(\text{OH})$) disappeared after acid activation with HCl solution, furthermore, the strong signals of iron chloride hydrate ($\text{FeCl}_3 \cdot 2\text{H}_2\text{O}$) were observed in the spectra. The acid activation process resulted in the conversion of hematite (Fe_2O_3) and goethite ($\text{FeO}(\text{OH})$) to iron chloride hydrate ($\text{FeCl}_3 \cdot 2\text{H}_2\text{O}$). After acid activation, iron chloride hydrate ($\text{FeCl}_3 \cdot 2\text{H}_2\text{O}$) and gibbsite ($\text{Al}(\text{OH})_3$) became the dominant phases, which accorded with the evidence of FTIR spectra change. Moreover, the mineralogical inhomogeneity and intensity of Bauxsol decreased after acid activation (as shown in Fig. 2). Freire et al. (2012) and Genç-Fuhrman et al. (2004) demonstrated that the dissolution of partial minerals after acid activation led to the increased surface area and higher anion adsorption capacity.

3.2. Central composite design and polynomial model for phosphate removal by acid-activated Bauxsol

Table 3 shows the experimental design and results based on CCD. The polynomial model was attained as Eq. (5):

Table 1
Surface property of Bauxsol before and after acid activation.

Sample	BET surface area ($\text{m}^2 \text{ g}^{-1}$)	Micropore area ($\text{m}^2 \text{ g}^{-1}$)	Mesopore area ($\text{m}^2 \text{ g}^{-1}$)	Total pore volume ($\text{cm}^3 \text{ g}^{-1}$)
Bauxsol	40.67	16.00	24.67	0.045
Acid-activated Bauxsol	80.63	12.94	67.69	0.064

Table 2
Chemical composition of Bauxsol samples before and after acid activation.

Constituent	Bauxsol before acid activation (wt.%)	Bauxsol after acid activation (wt.%)
Fe ₂ O ₃	47.13	33.88
Al ₂ O ₃	23.62	30.96
Na ₂ O	8.35	3.83
SiO ₂	9.12	15.52
TiO ₂	7.51	14.69
CaO	2.38	0.54
Cr ₂ O ₃	0.18	0.23
MnO	0.14	0.06
K ₂ O	0.05	0.10
CuO	0.03	0.01
NiO	0.01	0.02
MgO	1.49	0.17

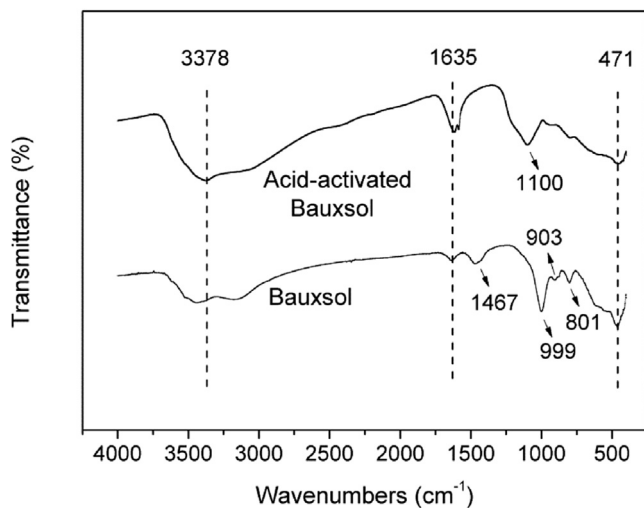


Fig. 1. FTIR spectra of Bauxsol before and after acid activation.

$$\begin{aligned} \text{Adsorption capacity} = & 192.20 - 9.34 \cdot \text{pH} + 2.17 \cdot \text{temperature} \\ & + 1.67 \cdot \text{pH} \cdot \text{temperature} - 36.17 \cdot \text{pH}^2 \\ & - 6.77 \cdot \text{temperature}^2 \end{aligned} \quad (5)$$

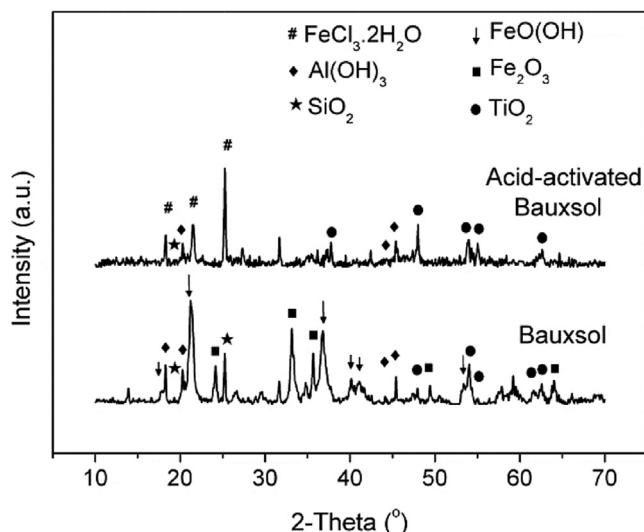


Fig. 2. XRD pattern of Bauxsol before and after acid activation.

The fitting quality was expressed by the coefficient of determination ($R^2 = 0.9729$), which provided a measure that how much variability in the observed response values could be explained by the experimental factors and their interactions (Zarei et al., 2010). In this study, the predicted R^2 of 0.9031 was reasonable consistent with the adjusted R^2 of 0.9535, which indicated that only 4.65% of the total variation could not be explained by the model. Furthermore, “Adeq Precision” indicated the ratio of signal to noise, and a ratio higher than 4 was desirable. The ratio of signal to noise was 20.085 in this study, indicating an adequate signal. Therefore, this model could be used to navigate the design space (Körbahti and Rauf, 2008).

Analysis of variance (ANOVA) for the experimental results from CCD model is shown in Table 4. The Model F -value of 50.26 implied that the RSM model was significant. The p -values are used to check the significance of each coefficient. The p -values less than 0.0500 indicate that the corresponding RSM model term is significant. In this study, pH, pH² and temperature² were significant model terms. Particularly, pH² ($p < 0.0001$) displayed the most significant effect on phosphate adsorption capacity, the Pareto value (P) of which reached 90.30%.

Fig. 3 shows the effects of initial solution pH and adsorption temperature on the phosphate adsorption onto acid-activated Bauxsol. The phosphate adsorption capacity firstly increased with the increase of pH, and then tended to decrease when the pH was higher than 4.5, which might be attributed to the different phosphorus species resulted from different pH (Youngran et al., 2007; Zhang et al., 2007). When the pH was below 3.0, phosphoric acid (H₃PO₄) was the main existence form, which was not very active in chemical adsorption. With the increase of pH, phosphorus species H₂PO₄⁻ and HPO₄²⁻ became the main existence forms, which were easily adsorbed onto the acid-activated Bauxsol. When the pH was higher than 4.5, the strong competition adsorption between OH⁻ and phosphate might occur (Zhao et al., 2012). Similar results were obtained by Castaldi et al. (2010). Besides this, the increased pH might weaken the affinity between phosphate ions (in solution) and functional group (on adsorbent surface), because the adsorption of OH⁻ on adsorbent surface could affect the electrostatic properties of adsorbent. Specifically, the increased pH might lead to the formation of a new charged counter-ion layer, making the adsorbent surface being a comparable lower affinity to phosphate, and further affected the adsorption capacity of acid-activated Bauxsol (Yao et al., 2013).

As shown in Fig. 3, the phosphate adsorption capacity of acid-activated Bauxsol firstly increased with the increase of adsorption temperature and then decreased. The adsorption temperature influenced the particle transport processes or particle collision rates because of viscosity change, and thus influenced mixing energy dissipated in water. With increasing the adsorption

Table 3
Central composite design matrix.

Run	pH		Temperature (°C)		Adsorption capacity (mg g ⁻¹)		
	Uncoded	Coded	Uncoded	Coded	Experimental	Predicted	Residuals
1	0.96	-1.414	50.00	0	127.20	133.08	-5.88
2	8.04	+1.414	50.00	0	108.80	106.67	2.13
3	4.50	0	50.00	0	182.80	192.21	-9.41
4	4.50	0	50.00	0	197.80	192.21	5.59
5	4.50	0	50.00	0	192.80	192.21	0.59
6	4.50	0	50.00	0	188.80	192.21	-3.41
7	4.50	0	50.00	0	198.80	192.21	6.59
8	7.00	+1	65.00	+1	143.80	143.79	0.01
9	2.00	-1	65.00	+1	164.80	159.13	5.67
10	7.00	+1	35.00	-1	134.13	136.10	-1.97
11	2.00	-1	35.00	-1	161.80	158.10	3.70
12	4.50	0	28.79	-1.414	175.13	175.60	-0.47
13	4.50	0	71.21	+1.414	178.47	181.76	-3.29

Table 4
Analysis of variance (ANOVA) for experimental results from CCD model.

Source	Sum of squares	df	Mean square	F-Value	p-value Prob > F	Remark
Model	9875.21	5	1975.04	50.26	<0.0001	Significant
pH	697.29	1	697.29	17.74	0.0040	
Temperature	37.76	1	37.76	0.96	0.3596	
pH*Temperature	11.11	1	11.11	0.28	0.6114	
pH ²	9099.32	1	9099.32	231.55	<0.0001	
Temperature ²	318.52	1	318.52	8.11	0.0248	
Residual	275.08	7	39.30			

temperature, the viscosity decreased and the rapid-mixing conditions could lead to homogeneous distribution of metal species, which resulted in acceleration of dissolution, hydrolysis, polymerization and adsorption reactions, and further better phosphate adsorption capacity of acid-activated Bauxsol (Wei et al., 2009; Chiang et al., 2001). However, the adsorption stability between acid-activated Bauxsol and phosphate decreased with increasing the adsorption temperature.

A multiple response method with Design-Expert V8.0 was applied for optimizing the combination of initial solution pH, adsorption temperature and phosphate adsorption capacity. Within the initial solution pH from 2.00 to 7.00, adsorption temperature from 35.00 to 65.00 °C, the numerical optimization was applied to maximize the phosphate adsorption capacity. As shown in Fig. 4, a maximum predicted phosphate adsorption capacity of

192.94 mg g⁻¹ was achieved at an initial solution pH of 4.19 and an adsorption temperature of 52.18 °C, which increased by 7.61 times compared with that of Bauxsol (22.40 mg g⁻¹) and was higher than other red mud adsorbents (as shown in Table 5).

3.3. Desorption behaviours

Desorption process not only recover the useful resource, but also regenerate the adsorbents simultaneously, which minimizes the cost for adsorbent replacement. As shown in Fig. 5, the phosphate desorption efficiency of acid-activated Bauxsol was as high as 94.16% in the first adsorption–desorption cycle, which still maintained 93.02% in the fifth cycle. Meanwhile, the adsorption capacity of acid-activated Bauxsol was 150.26 mg g⁻¹ in the fifth cycle, which maintained 80.48% of the maximum phosphate adsorption capacity. The results demonstrated that the acid-activated Bauxsol was successfully regenerated and repeatedly used in the wastewater treatment with high phosphate concentration.

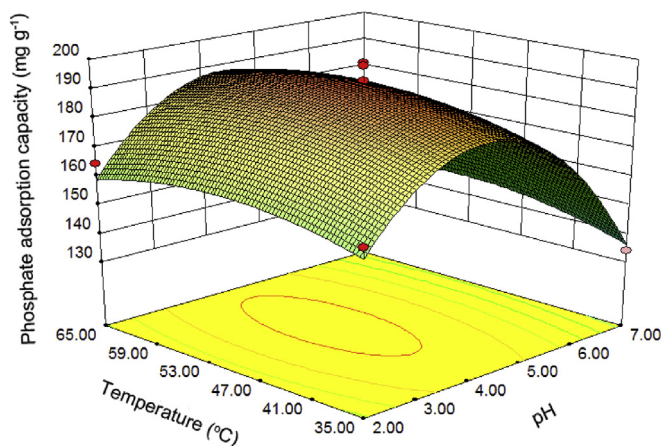


Fig. 3. Effects of initial solution pH and adsorption temperature on phosphate adsorption capacity of acid-activated Bauxsol.

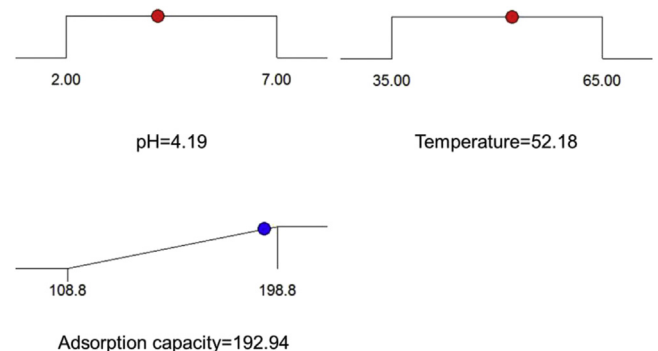


Fig. 4. Desirability ramp for numerical optimization of three goals: pH, temperature and phosphate adsorption capacity.

Table 5
Comparison of phosphate adsorption capacities of various red mud adsorbents.

Adsorption material	Initial phosphate concentration (mg L ⁻¹)	pH	Temperature (°C)	Dosage (g L ⁻¹)	Phosphate adsorption capacity (mg g ⁻¹)	References
Raw red mud	25.00	3.00	20.00	1.50	16.27	Zhao et al., 2009
HCl activated red mud	3.06	5.50	40.00	1.00	1.78	Huang et al., 2008
HCl activated red mud	475.00	7.00	25.00	5.00	94.05	Li et al., 2006
HCl activated red mud	3.20	7.50	–	0.07	38.67	Zhao et al., 2011
Bauxsol	142.50	6.20	23.00	2.00	3.21	Akhurst et al., 2006
HCl activated Bauxsol	200.00	4.19	52.18	0.50	192.94	This study

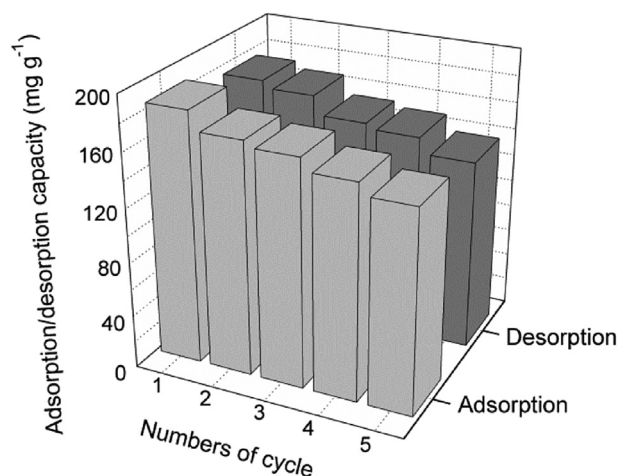


Fig. 5. Effect of Adsorption–desorption cycles on phosphate adsorption capacity and desorption efficiency of acid-activated Bauxsol.

4. Conclusion

- (1) The acid activation process led to the conversion of hematite (Fe₂O₃) and goethite (FeO(OH)), iron chloride hydrate (FeCl₃·2H₂O) and gibbsite (Al(OH)₃) became the dominant phases of acid-activated Bauxsol adsorption. Meanwhile, the cleaning of effective adsorption sites on the surface and decrease of the mineralogical inhomogeneity and intensity of Bauxsol after acid activation resulted in a higher BET surface area and total pore volume.
- (2) Acid-activated Bauxsol was successfully used for wastewater treatment with high phosphate concentration. Maximum phosphate adsorption capacity of 192.94 mg g⁻¹ was achieved at an initial solution pH of 4.19 and an adsorption temperature of 52.18 °C by acid-activated Bauxsol, which increased by 7.61 times compared with that of Bauxsol (22.40 mg g⁻¹), and was higher than other red mud adsorbents.
- (3) Acid-activated Bauxsol was successfully regenerated and repeatedly used in wastewater treatment with high phosphate concentration.

Acknowledgments

The authors are thankful to the CSC (China Scholarship Council), the National Natural Science Foundation of China (51178047, 51378190, 51039001), and Furong Scholar of Hunan Province for supporting.

Appendix A. Supplementary data

Supplementary data related to this article can be found at <http://dx.doi.org/10.1016/j.jenvman.2015.11.023>.

References

- Akhurst, D.J., Jones, G.B., Clark, M., McConchie, D., 2006. Phosphate removal from aqueous solutions using neutralised Bauxite refinery residues (Bauxsol™). *Environ. Chem.* 3, 65–74.
- Bezerra, M.A., Santelli, R.E., Oliveira, E.P., Villar, L.S., Escalera, L.A., 2008. Response surface methodology (RSM) as a tool for optimization in analytical chemistry. *Talanta* 76, 965–977.
- Bhatnagar, A., Vilar, V.J.P., Botelho, C.M.S., Boaventura, R.A.R., 2011. A review of the use of red mud as adsorbent for the removal of toxic pollutants from water and wastewater. *Environ. Technol.* 32, 231–249.
- Castaldi, P., Silveti, M., Garau, G., Deiana, S., 2010. Influence of the pH on the accumulation of phosphate by red mud (a bauxite ore processing waste). *J. Hazard. Mater.* 182, 266–272.
- Chiang, Y.C., Chiang, P.C., Huang, C.P., 2001. Effects of pore structure and temperature on VOC adsorption on activated carbon. *Carbon* 39, 523–534.
- Chowdhury, P., Viraraghavan, T., Srinivasan, A., 2010. Biological treatment processes for fish processing wastewater—a review. *Bioresour. Technol.* 101, 439–449.
- Desai, K.M., Survase, S.A., Saudagar, P.S., Lele, S.S., Singhal, R.S., 2008. Comparison of artificial neural network (ANN) and response surface methodology (RSM) in fermentation media optimization: case study of fermentative production of scleroglucan. *Biochem. Eng. J.* 41, 266–273.
- Despland, L.M., Clark, M.W., Aragno, M., Vancov, T., 2010. Minimising alkalinity and pH spikes from Portland cement-bound Bauxsol (seawater-Bauxsol) pellets for pH circum-neutral waters. *Environ. Sci. Technol.* 44, 2119–2125.
- Freire, T.S.S., Clark, M.W., Comarmond, M.J., Payne, T.E., Reichelt-Brushett, A.J., Thorogood, G.J., 2012. Electroacoustic isoelectric point determinations of bauxite refinery residues: different neutralisation techniques and minor mineral effects. *Langmuir* 28, 11802–11811.
- Gadepalle, V.P., Ouki, S.K., Herwijnen, V.R., Hutchings, T., 2007. Immobilization of heavy metals in soil using natural and waste materials for vegetation establishment on contaminated sites. *Soil Sediment. Contam.* 16, 233–251.
- Geç-Fuhrman, H., Bregnhøj, H., McConchie, D., 2005. Arsenate removal from water using sand–red mud columns. *Water Res.* 39, 2944–2954.
- Geç-Fuhrman, H., Tjell, J.C., McConchie, D., 2004. Increasing the arsenate adsorption capacity of Bauxsol (Bauxsol). *J. Colloid Interf. Sci.* 271, 313–320.
- Gok, A., Omastova, M., Prokes, J., 2007. Synthesis and characterization of red mud/polyaniline composites: electrical properties and thermal stability. *Eur. Polym. J.* 43, 2471–2480.
- Gong, J.L., Wang, B., Zeng, G.M., Yang, C.P., Niu, C.G., Niu, Q.Y., Zhou, W.J., Liang, Y., 2009. Removal of cationic dyes from aqueous solution using magnetic multi-wall carbon nanotube nanocomposite as adsorbent. *J. Hazard. Mater.* 164, 1517–1522.
- Haaland, D.P., 1989. *Experimental Design in Biotechnology*. Marcel Dekker, Inc., New York, Basel.
- Hatambeygi, N., Abedi, G., Talebi, M., 2011. Method development and validation for optimised separation of salicylic, acetyl salicylic and ascorbic acid in pharmaceutical formulations by hydrophilic interaction chromatography and response surface methodology. *J. Chromatogr. A* 1218, 5995–6003.
- Huang, W., Wang, S., Zhu, Z., Li, L., Yao, X., Rudolph, V., Haghseresht, F., 2008. Phosphate removal from wastewater using red mud. *J. Hazard. Mater.* 158, 35–42.
- Ivanova, E., Hadjiivanov, K., Klissurski, D., Bevilacqua, M., Armaroli, T., Busca, G., 2001. FTIR study of species arising after NO adsorption and NO+O₂ co-adsorption on CoY: comparison with Co-ZSM-5. *Micropor. Mesopor. Mater.* 46, 299–309.
- Jangir, D.K., Tyagi, G., Mehrotra, R., Kundu, S., 2010. Carboplatin interaction with calf thymus DNA: a FTIR spectroscopic approach. *J. Mol. Struct.* 969, 126–129.
- Körbahti, B.K., Rauf, M.A., 2008. Response surface methodology (RSM) analysis of photoinduced decoloration of toluidine blue. *Chem. Eng. J.* 136, 25–30.
- Kunamneni, A., Singh, S., 2005. Response surface optimization of the separation of enzymatic hydrolysis of maize starch for higher glucose production. *Biochem. Eng. J.* 27, 179–190.
- Li, Y., Liu, C., Luan, Z., Peng, X., Zhu, C., Chen, Z., Zhang, Z., Fan, J., Jia, Z., 2006. Phosphate removal from aqueous solutions using raw and activated red mud and fly ash. *J. Hazard. Mater.* 137, 374–383.
- Liu, W., Yang, J., Xiao, B., 2009. Application of Bayer red mud for iron recovery and building material production from aluminosilicate residues. *J. Hazard. Mater.* 161, 474–478.
- Lombi, E., Zhao, F.J., Zhang, G.Y., Sun, B., Fitz, W., Zhang, H., McGrath, S.P., 2002. In

- situ fixation of metals in soils using bauxite residue: chemical assessment. *Environ. Pollut.* 118, 435–443.
- Long, F., Gong, J.L., Zeng, G.M., Chen, L., Wang, X., Deng, J., Niu, Q., Zhang, H., Zhang, X., 2011. Removal of phosphate from aqueous solution by magnetic Fe–Zr binary oxide. *Chem. Eng. J.* 171, 448–455.
- Oguz, E., 2004. Removal of phosphate from aqueous solution with blast furnace slag. *J. Hazard. Mater.* 114, 131–137.
- Pariikh, S.J., Chorover, J., 2006. ATR-FTIR spectroscopy reveals bond formation during bacterial adhesion to iron oxide. *Langmuir* 22, 8492–8500.
- Pérez-Villarejo, L., Corpas-Iglesias, F.A., Martínez-Martínez, S., Artiaga, R., Pascual-Cosp, J., 2012. Manufacturing new ceramic materials from clay and red mud derived from the aluminium industry. *Constr. Build. Mater.* 35, 656–665.
- Savii, C., Popovici, M., Enache, C., Subrt, J., Niznansky, D., Bakardzieva, S., Caizer, C., Hrianea, I., 2002. Fe₂O₃–SiO₂ composites obtained by sol–gel synthesis. *Solid State Ionics* 151, 219–227.
- Shao, X., Peng, D., Teng, Z., Ju, X., 2008. Treatment of brewery wastewater using anaerobic sequencing batch reactor (ASBR). *Bioresour. Technol.* 99, 3182–3186.
- Siriwardane, R.V., Robinson, C., Shen, M., Simonyi, T., 2007. Novel regenerable sodium-based sorbents for CO₂ capture at warm gas temperatures. *Energy Fuels* 21, 2088–2097.
- Sohsalam, P., Sirianuntapiboon, S., 2008. Feasibility of using constructed wetland treatment for molasses wastewater treatment. *Bioresour. Technol.* 99, 5610–5616.
- Talebpour, Z., Ghassempour, A., Abbaci, M., Aboul-Enein, H.Y., 2009. Optimization of microwave-assisted extraction for the determination of glycyrrhizin in menthazin herbal drug by experimental design methodology. *Chromatographia* 70, 191–197.
- Tor, A., Cengeloglu, Y., Ersoz, M., 2009. Increasing the phenol adsorption capacity of neutralized red mud by application of acid activation procedure. *Desalination* 242, 19–28.
- Wei, L., Qiu, H., Zhang, J., Yu, Y., Yang, K., Liu, Z., Ding, G., 2009. Characteristic of a novel composite inorganic polymer coagulant-PFAC prepared by hydrochloric pickle liquor. *J. Hazard. Mater.* 162, 174–179.
- Weng, L., Vega, F.A., Riemsdijk, W.H.V., 2011. Competitive and synergistic effects in pH dependent phosphate adsorption in soils: LCD modeling. *Environ. Sci. Technol.* 45, 8420–8428.
- Xu, P., Zeng, G.M., Huang, D.L., Feng, C.L., Hu, S., Zhao, M.H., Lai, C., Wei, Z., Huang, C., Xie, G.X., Liu, Z.F., 2012. Use of iron oxide nanomaterials in wastewater treatment: a review. *Sci. Total Environ.* 424, 1–10.
- Yang, J., Zhang, D., Hou, J., He, B., Xiao, B., 2008. Preparation of glass-ceramics from red mud in the aluminium industries. *Ceram. Int.* 34, 125–130.
- Yao, Y., Gao, B., Chen, J., Yang, L., 2013. Engineered biochar reclaiming phosphate from aqueous solutions: mechanisms and potential application as a slow-release fertilizer. *Environ. Sci. Technol.* 47, 8700–8708.
- Ye, J., Zhang, P., Hoffmann, E., Zeng, G., Tang, Y., Dresely, J., Liu, Y., 2014. Comparison of response surface methodology and artificial neural network in optimization and prediction of acid activation of Bauxsol for phosphorus adsorption. *Water Air Soil Pollut.* 225, 2225.
- Youngran, J., Fan, M., Leeuwen, J.V., Belczyk, J.F., 2007. Effect of competing solutes on arsenic(V) adsorption using iron and aluminum oxides. *J. Environ. Sci.* 19, 910–919.
- Yu, H.G., Zhang, H.L., Wang, X.M., Gu, Z.W., Li, X.D., Deng, F., 2007. Local structure of hydroxy–peroxy apatite: a combined XRD, FT-IR, Raman, SEM, and solid-state NMR study. *J. Phys. Chem. Solids* 68, 1863–1871.
- Yue, Q., Zhao, Y., Li, Q., Li, W., Gao, B., Han, S., Qi, Y., Yu, H., 2010. Research on the characteristics of red mud granular adsorbents (RMGA) for phosphate removal. *J. Hazard. Mater.* 176, 741–748.
- Zarei, M., Niaei, A., Salari, D., Khataee, A., 2010. Application of response surface methodology for optimization of peroxi-coagulation of textile dye solution using carbon nanotube-PTFE cathode. *J. Hazard. Mater.* 173, 544–551.
- Zhang, G., Qu, J., Liu, H., Liu, R., Wu, R., 2007. Preparation and evaluation of a novel Fe–Mn binary oxide adsorbent for effective arsenite removal. *Water Res.* 41, 1921–1928.
- Zhang, T., Ding, L., Ren, H., Guo, Z., Tan, J., 2010. Thermodynamic modeling of ferric phosphate precipitation for phosphorus removal and recovery from wastewater. *J. Hazard. Mater.* 176, 444–450.
- Zhao, Y., Wang, J., Luan, Z., Peng, X., Liang, Z., Shi, L., 2009. Removal of phosphate from aqueous solution by red mud using a factorial design. *J. Hazard. Mater.* 165, 1193–1199.
- Zhao, Y., Yue, Q., Li, Q., Li, Q., Gao, B., Han, S., Yu, H., 2012. Influence of sintering temperature on orthophosphate and pyrophosphate removal behaviors of red mud granular adsorbents (RMGA). *Colloids Surf. A Physicochem. Eng. Asp.* 394, 1–7.
- Zhao, Y., Zhang, L., Ni, F., Xi, B., Xia, X., Peng, X., Luan, Z., 2011. Evaluation of a novel composite inorganic coagulant prepared by red mud for phosphate removal. *Desalination* 273, 414–420.
- Zhou, J., Yang, S., Yu, J., Shu, Z., 2011. Novel hollow microspheres of hierarchical zinc–aluminum layered double hydroxides and their enhanced adsorption capacity for phosphate in water. *J. Hazard. Mater.* 192, 1114–1121.